3. B. Hedtke, T. Börner, A. Weihe, *Science* **277**, 809 (1997).
4. D. L. Ollis, P. Brick, R. Hamlin, N. G. Xuong, T. A. Steitz, *Nature* **313**, 762 (1985).
5. C. A. Brautigam and T. A. Steitz, *Curr. Opin. Struct. Biol.* **8**, 54 (1998).
6. T. A. Steitz, S. J. Smerdon, J. Jäger, C. M. Joyce, *Science* **266**, 2022 (1994).
7. P. H. von-Hippel, D. G. Bear, W. D. Morgan, J. A. McSwiggen, *Annu. Rev. Biochem.* **53**, 389 (1984).
8. A. J. Carpousis and J. D. Gralla, *Biochemistry* **19**, 3245 (1980).
9. R. A. Ikeda and C. C. Richardson, *Proc. Natl. Acad. Sci. U.S.A.* **83**, 3614 (1986).
10. G. M. T. Cheetham, D. Jeruzalmi, T. A. Steitz, *Nature* **399**, 80 (1999).
11. S. Doublié, S. Tabor, A. M. Long, C. C. Richardson, T. Ellenberger, *Nature* **391**, 251 (1998).
12. D. Jeruzalmi and T. A. Steitz, *EMBO J.* **17**, 4101 (1998).
13. Crystals of the quaternary complex reported here were grown similarly to those of the binary complex described previously (*10*); T7 RNAP was mixed (0.3 mM) with a T7 promoter (0.35 mM), in the presence of ribonucleotides GTP, uridine 5′-triphosphate, cytidine 5′-triphosphate, and α,β-methylene ATP (4 mM each) and 15 mM $MgCl_2$. The promoter was constructed by annealing together two synthetic oligonucleotides that consisted of a 22-nt template strand of sequence 5′-CTCCCTATAGTGAGTCGTATTA-3′ and a 17-nt nontemplate strand of sequence 5′-TAATACGACTCACTATA-3′. This produced a 17–base pair duplex and a 5-nt template overhang. In this way, the T7 RNAP synthesized a 3-nt RNA and stopped at position +4 of the template strand before crystallization. Data were collected at Brookhaven National Laboratory (station X25), using x-rays of wavelength 1.10 Å, which were recorded with a Brandeis B4 charge-coupled device detector and reduced with the program MOSFLM (*34*). The crystals are orthorhombic space group $P2_12_12$ with cell dimensions of a = 221.2 Å, b = 73.6 Å, and c = 80.9 Å. The number of unique reflections recorded was 51,537 (97.8% complete, with 40 to 2.4 Å resolution), with an overall multiplicity of 3.8 and a crystallographic R factor for merging all data (40 to 2.4 Å), R_{merge}, of 0.078. Subsequent analysis was performed with the CCP4 software suite (*35*). Despite an R factor of 24% between these data and data from the T7 RPP complex, the template strand 5′-overhang and 5′-pppGpGpG-3′ RNA transcript could clearly be seen in difference Fourier maps calculated with the observed amplitudes from the two crystals and phases derived from the T7 RPP coordinates. The initial crystallographic R factor for the completed model was 0.40 (R_{free} = 0.42). Model refinement (*36*) and rebuilding (*37*) reduced the R factor to 0.22 (R_{free} = 0.26) for all data at a 40 to 2.4 Å resolution; $F > 2\sigma(F)$.
14. The absence of α,β-methylene ATP in these crystals may have resulted from its loss by diffusion when the crystals were soaked in cryoprotection solution: The Michaelis constant K_m for the interaction between T7 RNAP and the NTP in the incoming binding site is ~0.1 mM, determined for optimized in vitro transcription conditions (*38*), and α,β-methylene ATP has poor solubility at high concentrations of polyethyleneglycol/propyleneglycol solution. Alternatively, however, the conformation of the enzyme in this crystal form may play an important role in determining the captured transcription intermediate. Several other crystals that diffracted to a resolution of 2.8 Å clearly have bound magnesium ions and partially occupied α,β-methylene ATP at the +4 position in the active site. In this instance, the template strand and residue Tyr^{639} appear to be poorly ordered in electron density maps.
15. L. A. Kohlstaedt, J. Wang, J. M. Friedman, P. A. Rice, T. A Steitz, *Science* **256**, 1783 (1992).
16. J. Wang *et al.*, *Cell* **89**, 1087 (1997).
17. Y. Li, S. Korolev, G. Waksman, *EMBO J.* **17**, 7514 (1998).
18. G. Gao, M. Orlova, M. M. Georgiadis, W. A. Hendrickson, S. P. Goff, *Proc. Natl. Acad. Sci. U.S.A.* **94**, 407 (1997).
19. J. R. Kiefer, C. Mao, J. C. Braman, L. S. Beese, *Nature* **391**, 304 (1998).
20. R. Sousa and R. Padilla, *EMBO J.* **14**, 4609 (1995).
21. M. Astatke, N. D. F. Grindley, C. M. Joyce, *J. Biol. Chem.* **270**, 1945 (1995).
22. V. O. Rechinsky, D. A Kostyuk, V. L. Tunitskaya, S. N. Kochetkov, *FEBS Lett.* **306**, 129 (1992).
23. H. Huang, R. Chopra, G. L. Verdine, S. C. Harrison, *Science* **282**, 1669 (1998).
24. S. H. Eom, J. Wang, T. A. Steitz, *Nature* **382**, 278 (1996).
25. A. H. Wang *et al.*, *Nature* **299**, 601 (1982).
26. T. A. Steitz, *J. Biol. Chem.* **274**, 17395 (1999).
27. R. Sousa, Y. J. Chung, J. P. Rose, B.-C. Wang, *Nature* **364**, 595 (1993).
28. P. A. Osumi-Davis, M. C. Aguilera, R. W. Woody, A. Y. M. Woody, *J. Mol. Biol.* **226**, 37 (1992).
29. L. P. Gardner, K. A. Mookhtiar, J. E. Coleman, *Biochemistry* **36**, 2908 (1997).
30. J. Villemain and R. Sousa, *J. Mol. Biol.* **281**, 793 (1998).
31. J. Lykke-Andersen and J. Christiansen, *Nucleic Acids Res.* **26**, 5630 (1998).
32. C. T. Martin, D. K. Muller, J. E. Coleman, *Biochemistry* **27**, 3966 (1988).
33. B. M. Matthews, *J. Mol. Biol.* **33**, 491 (1968).
34. A. G. W. Leslie, *Joint CCP4 and ESF-EACMB Newsletter Protein Crystallography No. 26* (Daresbury Laboratory, Warrington, UK, 1992).
35. Collaborative Computational Project No. 4, *Acta Crystallogr.* **D50**, 760 (1994).
36. A. T. Brünger et al., *Acta Crystallogr.* **D54**, 905 (1998).
37. T. A Jones, J. Y. Zou, S. W. Cowan, M. Kjeldgaard, *Acta Crystallogr.* **A47**, 110 (1991).
38. J. L. Oakley, R. E. Strothkamp, A. H. Sarris, J. E. Coleman, *Biochemistry* **18**, 528 (1979).
39. M. Carson, *J. Appl. Crystallogr.* **24**, 958 (1991).
40. Single-letter abbreviations for the amino acid residues are as follows: D, Asp; E, Glu; F, Phe; G, Gly; H, His; K, Lys; M, Met; Q, Gln; R, Arg; W, Trp; and Y, Tyr.
41. A. Nicholls, R. Bharadwaj, B. Honig, *Biophys. J.* **64**, A166 (1993).

42. We thank J. Ippolito, D. Kennedy, and J. Wang for discussions and P. Eatherton for assistance in the preparation of this manuscript. This research was supported by NIH grant number GM-22778 (T.A.S.). The complete refined coordinates of the T7 RNAP transcribing complex and the observed structure factor amplitudes have been deposited in the Protein Data Bank with numbers 1QLN and R1QLNSF.

5 October 1999; accepted 15 November 1999

REPORTS

Phase-Coherent Amplification of Matter Waves

Mikio Kozuma,[1] Yoichi Suzuki,[1] Yoshio Torii,[2] Toshiaki Sugiura,[1] Takahiro Kuga,[1] E. W. Hagley,[3] L. Deng[3]

Phase-coherent matter-wave amplification was demonstrated using Bose-Einstein–condensed rubidium-87 atoms. A small seed matter wave was created with coherent optical Bragg diffraction. Amplification of this seed matter wave was achieved by using the initial condensate as a gain medium through the superradiance effect. The coherence properties of the amplified matter wave, studied with a matter-wave interferometer, were shown to be locked to those of the initial seed wave. The active matter-wave device demonstrated here has great potential in the fields of atom optics, atom lithography, and precision measurements.

Advances in laser science and technology have been supported by the development of a variety of optical elements that can be categorized as either passive or active. Mirrors, beam splitters, and polarizers are typical examples of passive elements, whereas devices such as optical pulsed-dye amplifiers (*1*) are active ones. By passing through such an active device, a weak laser beam can be amplified while maintaining its phase coherence: the mechanism of lasing itself.

In the field of atom optics it has long been speculated, in direct analogy with optical amplifiers, that it should be possible to coherently amplify a matter wave by using an appropriate gain medium. Bose-Einstein condensation (the macroscopic occupation of a single quantum state) in dilute alkali gases (*2, 3*) has the potential of being such a gain medium because it is an ideal source of highly coherent matter waves. What has long since happened for the optical laser is now becoming a reality for matter waves. In fact, many passive matter-wave elements have already been demonstrated. For example, Bragg diffraction (*4*) of a Bose-Einstein condensate (BEC) by a moving, optical standing wave (*5*) can be used to coherently diffract any fraction of a BEC into a selectable momentum state, making it an ideal mirror or beam splitter. These passive elements were key in the development of a highly efficient (nearly 100% contrast) Mach-Zehnder BEC interferometer (*6, 7*). In addition, most

[1]Institute of Physics, University of Tokyo, 3-8-1 Komaba, Meguro-ku, Tokyo 153-8902, Japan. [2]Department of Physics, Gakushuin University, Mejiro 1-5-1, Toshima-ku, Tokyo 171-8588, Japan. [3]Physics Lab, National Institute of Standards and Technology, Gaithersburg, MD 20899, USA.

BEC atom lasers (*8*–*11*) demonstrated thus far rely on changing the internal spin state of the atoms, and this can be thought of as a passive matter-wave polarizer. What is lacking in this otherwise complete group of passive atom-optic elements are active ones.

An atom-light interaction that holds the key to the development of such an active element was recently observed. This process, called superradiance (*12*), occurs when a nonspherical condensate is illuminated by off-resonant laser light. Spontaneous emission initially causes atoms to scatter randomly into various momentum states. These scattered matter waves interfere with the condensate, forming a moving matter-wave grating that further scatters the laser beam. Because the condensate is not spherical, specific matter-wave gratings grow and become dominant (*12*). The spontaneous emission process (normal Rayleigh scattering) gives way to a coherent process whose rate grows as the depth of the matter-wave grating increases. The process is self-amplifying because every scattered photon creates another recoiling atom that increases the amplitude of the matter-wave grating. This can be thought of as a stimulated matter-wave generator, in analogy with parametric generation in optical laser systems. However, because the process starts from spontaneously generated noise, the phase of the atomic grating is not controllable. Furthermore, there has been no experimental evidence as to whether this superradiant element maintains the long-range coherence properties of the condensate.

Here we report the first demonstration of an active, phase-coherent, matter-wave amplifier (*13*). Instead of relying on spontaneously generated noise, we established a small, coherent atomic seed in the BEC in a high momentum state using optical Bragg diffraction (*5*). The superradiance effect was used solely as a gain medium. Clear evidence of the increase in the population of the seed matter wave was observed. We verified that the phase of the amplified matter wave was locked to that of the injected seed, using a new type of Mach-Zehnder interferometer (*7*).

The experiment was performed with a condensate of $\sim 2 \times 10^5$ ^{87}Rb atoms formed in a dc magnetic trap (*14*) with a standard evaporation technique (*2*). We first trapped about 10^9 atoms in an ultra–high vacuum cell using a double magneto-optical trap (*15*). The atoms were then transferred into a dc magnetic trap and were further cooled by radio frequency–induced evaporation. We created a BEC in the 5 $S_{1/2}$, F = 1, m = −1 state, in a trap with a radial gradient, axial curvature, and a bias field of 1.75 T/m, 185 T/m^2, and 10^{-4} T, respectively. The condensate in such a trap is highly elongated. After forming the BEC, we turned off the magnetic trap and waited long enough that the magnetic fields decayed completely away. We then applied superradiance or Bragg laser pulses or both (Fig. 1A). Both the superradiance pulse (pulse A in Fig. 1A) and the Bragg pair pulse (pulses B and C in Fig. 1A) were derived from an optically amplified, grating-stabilized diode laser. The spatial mode of the laser was purified by passing it through a single-mode optical fiber, and the intensity at the exit of the fiber was actively stabilized. The laser beams were detuned from the 5 $S_{1/2}$, F = 1 → 5 $P_{3/2}$ F′ = 2 transition by $\Delta/2\pi = -2$ GHz, had an intensity of 3 mW/cm^2, and were applied along the axial (long) direction of our cigar-shaped condensate. The intensity was determined experimentally from the measured 5.6-kHz two-photon Rabi oscillation frequency of the Bragg beams (*7*). Although the rate of spontaneous emission from such a beam is only 0.05 ms^{-1}, the noise floor of our optical amplifier caused this rate to be much higher. We measured the spontaneous emission rate to be ~1 ms^{-1} by fitting the decay of atoms in the condensate under normal Rayleigh scattering.

When only beam A was applied, the recoiled-atom growth rate from superradiance was (*12*)

$$\frac{dN_j}{dt} = \left[\frac{3}{8\pi} RN_0\Omega_j \sin^2\theta_j - L_j\right](N_j + 1) \quad (1)$$

N_0 is the initial number of atoms in the condensate and N_j is the number that recoiled into the jth mode. R is the single-atom Rayleigh scattering rate (proportional to the laser intensity), θ_j is the angle between the polarization of the incident light and the direction of light emission, Ω_j is the solid angle for light emission, and L_j is the loss term arising from the coherence time of the atomic grating. Because of the BEC aspect ratio, the dominant phase-matched grating causes photons to backscatter, and these atoms thereby acquire a momentum of $2\hbar k$ through superradiance. The choice of applying the laser along the axial direction only supports this single superradiance mode. Applying a single pulse A 500 μs after turning off the magnetic trap, when the BEC was still well elongated (Fig. 1B), resulted in the coherent buildup of the matter-wave grating because of spontaneous superradiance, and caused 62% of the atoms to be scattered into this $|2\hbar k\rangle$ momentum state.

In order to make a matter-wave amplifier, we must suppress this spontaneous superradiance. That is, only an injected seed matter wave should be amplified. To do this, we increased the time before applying pulse A after extinguishing the trap in order to change the aspect ratio of the condensate. The condensate profile became more spherical because of the mean-field–driven expansion, and thus there was less of a preferred grating direction. When we applied pulse A 1.8 ms after extinguishing the magnetic trap (Fig. 1C), the coherent buildup of atoms in the $|2\hbar k\rangle$ state was greatly suppressed (the condensate aspect ratio was reduced by a factor of 2, decreasing the gain term in Eq. 1 by a factor of 4).

Coherent Bragg diffraction created the small matter-wave seed that was used to test the amplification process. The Bragg pulse was formed by a pair of linearly polarized, counter-propagating laser beams of slightly different frequencies (*5*). The frequency difference between the two laser beams was chosen to fulfill a first-order Bragg diffraction condition that changes the momentum state of the atoms without changing their internal state. In our case, the atoms acquired a kinetic energy of 4 E_r ($E_r \approx h \times 3.8$ kHz is the ^{87}Rb single-photon recoil energy), and the necessary relative detuning was $\Delta\omega/2\pi = 15$ kHz. Figure 1D shows the result of diffracting 6.5% of the atoms into the

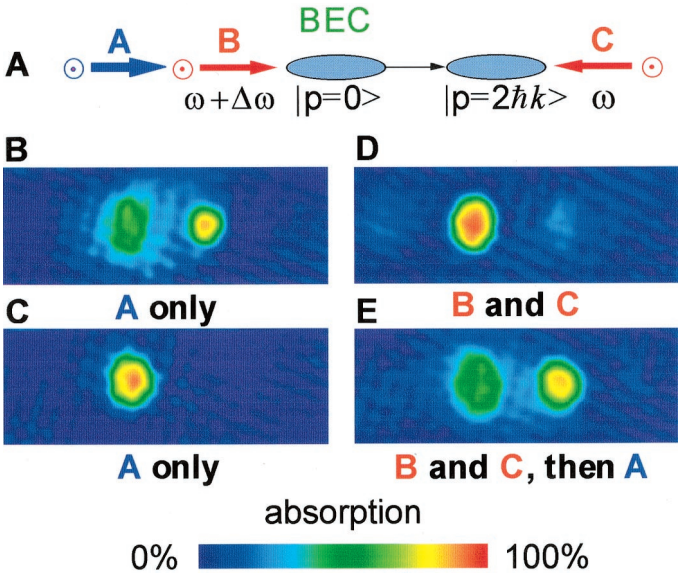

Fig. 1. (**A**) Direction along which the elongated condensate is illuminated by the superradiance (pulse A) and Bragg (pulses B and C) beams. (**B** through **E**) Absorption images showing the atomic momentum distribution 20 ms after the condensate was exposed to various laser pulses. The 20-ms time of flight (TOF) allows the momentum states enough time to separate completely in space. For these images, the width of the field of view is 940 μm by 350 μm, and the duration of pulse A is 520 μs.

$|2\hbar k\rangle$ state using a 15-μs Bragg diffraction pulse.

The amplification was accomplished by successive application of the seed Bragg pulse and of the superradiance pulse A, before the diffracted atoms left the region of the condensate. Applying the superradiance pulse A after creating the seed matter wave (Fig. 1E) produced a striking increase of atoms in the $|2\hbar k\rangle$ state to 66% of the original condensate number. The population of the injected coherent atomic matter wave was thereby amplified by more than a factor of 10. This increase can be seen in Fig. 2A, where population in the $|2\hbar k\rangle$ state is plotted as a function of the duration of the superradiance pulse A. At each pulse duration, no superradiance growth occurred without the injected seed (only normal Rayleigh scattering occurred). However, with the seed wave injected, the $|2\hbar k\rangle$ population increased as the duration of pulse A increased, allowing us to control the gain of the matter-wave amplifier. The case where the duration of pulse A was chosen so that at the end of the pulse pair there were equal numbers of atoms (50%) in each momentum state is shown in Fig. 2B.

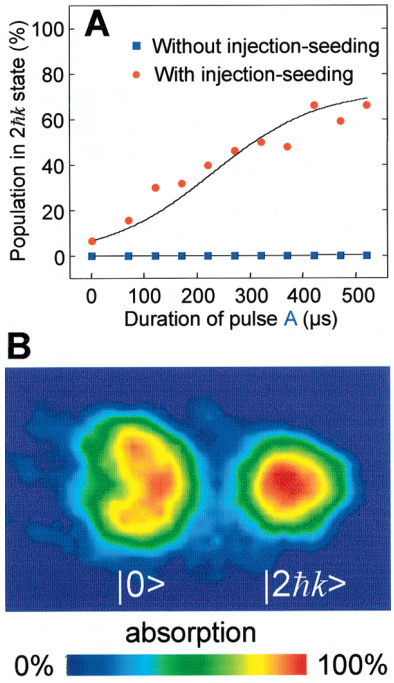

Fig. 2. (**A**) Population growth in the $|2\hbar k\rangle$ state is plotted as a function of the duration of pulse A both with (circles) and without (squares) the matter-wave seed. The solid curves are one-parameter fits (L_j) to Eq. 1. Here Ω_j is approximated to be λ^2/S, where S is the cross-sectional area of the condensate perpendicular to the direction of light emission, and λ is the optical wavelength. The best fit yielded $L_j = 3.8\ \mathrm{ms}^{-1}$ for both curves. (**B**) Absorption image taken after 15 ms TOF for a 50% split ratio. Although there are equal numbers of atoms in the two momentum states, their density distributions are not the same. The width of the field of view is 400 μm by 260 μm.

It is important to examine the coherence properties of this amplified wave. The phase coherence of the seed wave may have been completely lost by the amplification process, a phenomenon analogous to strongly amplified spontaneous emission (ASE) (*16*), frequently seen in optical pulsed-dye laser amplifiers that are not well aligned. We therefore needed to determine whether the long range coherence properties of the condensate were preserved in the amplification process and, if they were, whether the phase of the amplified matter wave followed that of the seed. In order to determine whether our amplified matter wave was phase-coherent, we studied its phase with a novel Mach-Zehnder interferometer (*7*) (Fig. 3).

We first applied a Bragg pulse to diffract 6.5% of the atoms into the $|2\hbar k\rangle$ state and then increased the population in this state to 50% of the initial condensate population, using superradiance amplification (Fig. 2B). The $|0\rangle$ and $|2\hbar k\rangle$ momentum states began to separate, and after 350 μs we applied a second (π) Bragg pulse. Because a π pulse inverts the two momentum states, the two spatially displaced clouds then began to converge. When the two clouds from the two different coordinate-space paths overlapped completely, we applied a third ($\pi/2$) Bragg pulse. If the long-range order were maintained for the amplified matter wave, and if the phase of this amplified wave followed that of the injected wave, the initial Bragg seed and superradiance pulse would together act as if they were a single, coherent, $\pi/2$ Bragg pulse. Consequently, the probability of finding atoms in the initial state $|0\rangle$ after all pulses had been applied would be unity (*7*) if the phase of the moving Bragg standing wave were not altered between pulses. If we then varied the phase φ of this moving standing wave just before the third ($\pi/2$) Bragg pulse was applied, the probability of finding atoms in the $|2\hbar k\rangle$ state would be $[1 - \cos(\varphi)]/2$ (*7*). The interferometer fringes mapped in this manner should have a contrast of 100%.

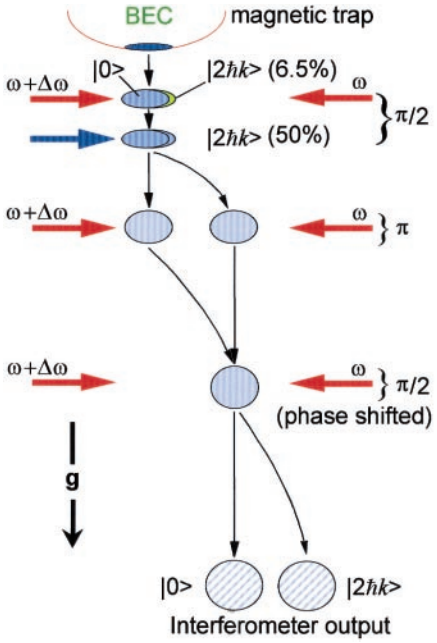

Fig. 3. Schematic of the Mach-Zehnder interferometer used to test the phase coherence of the amplified matter-wave seed.

However, if the long-range order were lost in the amplification process, we would expect to see a maximum interferometer contrast of only 36%, resulting from the interference between the initial seed wave and the rest of the condensate. If the long-range order were maintained for the amplified wave but the phase of the amplified wave was random with respect to the seed, the interferometer would not be stable because the probability of finding atoms in the $|2\hbar k\rangle$ state would fluctuate randomly from shot to shot. The coherence properties of the amplified matter wave are therefore integrally linked to the contrast of the interferogram.

We measured the interferometer contrast by varying the relative phase φ of the third ($\pi/2$) Bragg pulse in the range $0 < \varphi < 3.5\ \pi$. This was accomplished by changing the phase of one of the two Bragg beams composing the moving standing wave with an electro-optic modulator. After 20 ms of free evolution to allow the $|0\rangle$ and $|2\hbar k\rangle$ components enough time to separate significantly in space, an absorption image of the resulting condensate was taken. The $|2\hbar k\rangle$ state population oscillated as a function of φ (Fig. 4), and we observed an interference pattern with a contrast of 71(6)%. The facts that the fringe contrast exceeded 36% and that most of the atoms came back to the $|0\rangle$ state when $\varphi = 0$ are direct evidence that the long-range order was maintained and that the phase was locked to that of the seed matter wave. The contrast was not 100% because of the distortion of the atomic density distribution caused by the superradiance process. Superradiance is based on matter-wave bosonic stimulation, and thus the probability of superradiance is highest where the atomic density is greatest. Therefore, the atomic density

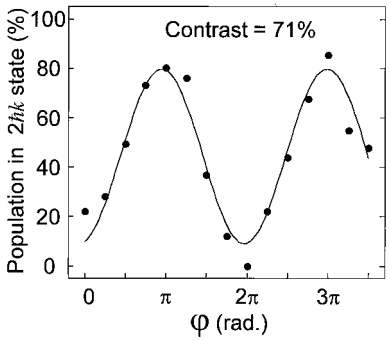

Fig. 4. Interferogram from the interferometer depicted in Fig. 3. The atomic population in the $|2\hbar k\rangle$ momentum state is plotted as a function of φ.

distributions of the two momentum states are not the same even though each momentum state contains the same total number of atoms (Fig. 2B). Consequently, when the two momentum states are combined with successive π and $\pi/2$ Bragg pulses, it is not possible to establish completely constructive or completely destructive interference. Three-dimensional numerical simulations that take into account the difference in the atomic density distributions (Fig. 2B) predict the maximum contrast to be 78%, which is in good agreement with our measured contrast of 71(6)%. This is to be compared to a Mach-Zehnder BEC interferometer (100% contrast) (*7*) that splits the condensate into two momentum states with identical density distributions, using a single $\pi/2$ Bragg pulse. The corrected maximum contrast of 78% implies that 83(14)% of the amplified wave is phase-coherent with the initial seed.

The phase-coherent matter-wave amplifier presented here is capable of amplifying a matter wave whose momentum p is in the range $0 < p < 2\hbar k$, provided the phase-matching condition is respected. If ϕ is the angle between the direction of propagation of the superradiance beam and that of the seed matter wave, the phase-matching condition becomes $p = 2\hbar k \cos\phi$. This condition is relaxed by the momentum spread of the source condensate, which, for a particular choice of ϕ, can be thought of as the matter-wave amplifier bandwidth.

In the present experiment, both the Bragg and the superradiance pulses were illuminated along the same direction. If we injected a small fraction of atoms along a different direction, we would be able to study mode competition in the matter-wave amplification process. One could use phase-coherent matter-wave amplification to enhance the number of atoms in atom lithography or holography (*17*) experiments in order to reduce signal accumulation time. Furthermore, it should be possible to make a ring cavity for matter waves using multiple Bragg diffractions as mirrors. By combining such a matter-wave cavity and the phase-coherent amplification mechanism demonstrated here, it should be possible to construct a new type of high-brightness atom laser.

References and Notes

1. B. G. Huth, *Appl. Phys. Lett.* **16**, 185 (1970).
2. M. H. Anderson *et al.*, *Science* **269**, 198 (1995).
3. K. B. Davis *et al.*, *Phys. Rev. Lett.* **75**, 3969 (1995).
4. P. J. Martin *et al.*, *Phys. Rev. Lett.* **60**, 515 (1988).
5. M. Kozuma *et al.*, *Phys. Rev. Lett.* **82**, 871 (1999).
6. D. M. Giltner, R. W. McGowan, S. A. Lee, *Phys. Rev. Lett.* **75**, 2638 (1995).
7. Y. Torii *et al.*, in preparation. Preprint available at http://xxx.lanl.gov/abs/cond-mat/9908160 (1999).
8. M.-O. Mewes *et al.*, *Phys. Rev. Lett.* **78**, 582 (1997).
9. B. P. Anderson and M. A. Kasevich, *Science* **282**, 1686 (1998). Unlike other atom lasers, in this work atoms in the same magnetic state tunnel out of a one-dimensional optical standing wave potential after the magnetic trap is switched off.
10. I. Bloch, T. W. Hänsch, T. Esslinger, *Phys. Rev. Lett.* **82**, 3008 (1999).
11. E. W. Hagley *et al.*, *Science* **283**, 1706 (1999).
12. S. Inouye *et al.*, *Science* **285**, 571 (1999).
13. C. K. Law and N. P. Bigelow, *Phys. Rev. A* **58**, 4791 (1998).
14. M.-O. Mewes *et al.*, *Phys. Rev. Lett.* **77**, 416 (1996).
15. C. J. Myatt *et al.*, *Opt. Lett.* **21**, 290 (1996).
16. G. I. Peters and L. Allen, *J. Phys. A* **4**, 238 (1971).
17. J. Fujita *et al.*, *Nature* **380**, 691 (1996).

18. Supported in part by a grant-in-aid from the Ministry of Education, Science, and Culture, and by Core Research for Evolutionary Science and Technology of the Japan Science and Technology Corporation. After submission of this manuscript, we learned that related work is being pursued at MIT.

28 September 1999; accepted 16 November 1999

Exciton Storage in Semiconductor Self-Assembled Quantum Dots

T. Lundstrom, W. Schoenfeld, H. Lee, P. M. Petroff*

Storage and retrieval of excitons were demonstrated with semiconductor self-assembled quantum dots (QDs). The optically generated excitons were dissociated and stored as separated electron-hole pairs in coupled QD pairs. A bias voltage restored the excitons, which recombined radiatively to provide a readout optical signal. The localization of the spatially separated electron-hole pair in QDs was responsible for the ultralong storage times, which were on the order of several seconds. The present limits of this optical storage medium are discussed.

Storing information in a cheap way will require ultrahigh packing densities as well as inexpensive self-assembling techniques and fast methods for writing and retrieving the information. Today, over 10 million atoms are required for storage of a single bit of information, but demands for faster addressing will require even smaller structures. Semiconductor QDs, which involve a few thousand atoms, may offer an attractive path toward achieving these goals. Charge storage devices based on the resistivity changes of a two-dimensional electron gas located near a layer of self-assembled QDs have been demonstrated at low temperature (*1, 2*). Quantum well (QW) devices designed for optical storage have been proposed and demonstrated (*3, 4*). Their storage characteristics are limited to short storage times (several hundred microseconds) at low temperature. Here, we present an approach for storing and retrieving information in QDs that uses an optical method and allows for exciton storage times of several seconds.

The QDs (*5*) are produced by molecular beam epitaxy (MBE). The size of the lens-shaped QDs (~30 to 40 nm in diameter and ~3 to 5 nm in height) is on the order of the electron wavelength, and the carrier energy levels are quantized. The sequential loading of electrons and holes and the three-dimensional confinement character of the carriers in the QDs have been demonstrated (*6*). The delta function density of states yields ultranarrow luminescence lines, and several studies have recently shown the importance and complexity of many body effects in the relaxation processes involved in strongly excited QDs (*7*).

The device structure of QDs presented here is based on the splitting of an optically generated exciton into an electron-hole pair for the write cycle. The electron and hole are stored in closely spaced strain-coupled QD pairs. The effects of this strain coupling are to locally lower the band gap of the material and to localize the electron-hole pair (*8*). After the electron and hole are stored for a given time, an applied voltage bias can bring them together in the same QD, where they recombine radiatively for the readout cycle. We show exciton storage times at low temperature, which are more than a billion times longer than the exciton lifetime in normal QDs.

The central part of the device structure contains an InAs QD layer and a narrow GaAs QW that are separated by a thin AlAs layer. The 7% lattice mismatch between InAs and GaAs creates a strain field around the coherently strained InAs QDs. This strain field extends through the thin AlAs barrier into the narrow GaAs QW, where it creates a buried strain-induced QD (SIQD) (*8*). The cross-sectional micrograph from a transmission electron microscope (TEM) (Fig. 1) indicates that the strain field of the InAs QD extends to the GaAs QW, where it gives rise to a strain contrast. The QW thickness is chosen to ensure that its lowest electron energy level is above the X valley minimum in the AlAs barrier. This approach allows one to engineer the ladder of electronic levels shown in Fig. 2. The cascaded energy level structure ensures that the excitons created in the QW are efficiently separated into electron-hole pairs under the influence of an electric field. The relaxation of the electron from the SIQD to the X valley is a rapid process that occurs in a few

Materials Department, University of California, Santa Barbara, CA 93106, USA.

*To whom correspondence should be addressed. E-mail: petroff@engineering.ucsb.edu